DOI: 10.1002/ejic.200700144

Tagging (Arene)ruthenium(II) Anticancer Complexes with Fluorescent Labels

Fabio Zobi,[a] Beeta Balali Mood,[a] Peter A. Wood,[a] Francesca P. A. Fabbiani,[a] Simon Parsons,[a] and Peter J. Sadler*[a]

Keywords: Anticancer agents / Organometallic compounds / Fluorescence / Ruthenium / Hydrolysis

Fluorescent (arene)ruthenium(II) complexes have been prepared by tagging a small fluorogenic reporter onto the chelating ligand of complexes of the type $[(\eta^6\text{-arene})RuCl(Z)]^+$ (Z = chelating ligand). Complexes $[(\eta^6\text{-}p\text{-cym})RuCl(NNO)](Cl)$ (**2**), $[(\eta^6\text{-}p\text{-cym})RuCl(\mathbf{L3})](Cl)$ (**3**) and $[(\eta^6\text{-}p\text{-cym})RuCl(\mathbf{L4})](Cl)$ (**4**) {*p*-cym = *p*-cymene, NNO = 2-[(2-aminoethyl)amino]ethanol, **L3** = 2-[(2-aminoethyl)amino]ethyl-2-(methylamino)benzoate and **L4** = *N*-{2-[(2-aminoethyl)-amino]ethyl}-2-(methylamino)benzamide} were obtained in good yield from the reaction of the Ru dimer $[(\eta^6\text{-}p\text{-cym})RuCl_2]_2$ (**1**) and the corresponding ligand. The compounds have been fully characterized and their X-ray crystal structures are reported. Compounds **3** and **4** show a photoluminescence response centered at 435 nm with partial fluorescence quenching of the fluorogenic reporters **L3** and **L4** upon coordination to the metal center. Species **2**–**4** show good solubility both in water and organic solvents. In water, **2**–**4** readily hydrolyze to form the aqua complexes. These are stable at acidic pH forming 10–15 % of the corresponding hydroxido complexes in buffered solution (25 mM HEPES) as the pH is raised to a physiological value (pH = 7.44). Under these conditions, **4** (but not **2** or **3**) undergoes a fast pH-dependent reversible intramolecular rearrangement. Experimental data and semiempirical calculations indicate that the major species arising from this transformation is a complex with a tridentate chelating ligand following deprotonation at the nitrogen atom of the amide group. Esterase-catalyzed hydrolysis of **3** liberates isatoic acid (**MIAH**) and generates **2** indicating that the complex is a substrate for the enzyme. Complexes similar to **3** may have potential for esterase-activated Ru-based prodrug delivery systems.

Introduction

Organometallic ruthenium(II) complexes of the type $[(\eta^6\text{-arene})RuCl(X)(Y)]$ (where X, Y are monodentate or chelating ligands) comprise a relatively new group of anticancer compounds which are cytotoxic to cancer cells, including cisplatin-resistant cell lines.[1,2] The geometry of the complexes is generally described as pseudo-octahedral "three-legged piano-stool" in which a π-bonded arene ligand provides the seat supported by a σ-bonded chlorido and a chelating ligand which form the three legs of the stool. The arene ligand is strongly bound and stabilizes the ruthenium(II) oxidation state. It resists hydrolysis and provides a lipophilic side to the complex.[3,4] Most of the halide compounds, however, are ionic and exhibit good aqueous solubility and appear to undergo rapid aquation (substitution of bound Cl by H_2O).[4] Thus, while η^6-arene–Ru^{II} bonds are inert toward hydrolysis, the monofunctional complexes $[(\eta^6\text{-arene})Ru^{II}(en)(Cl)]^+$ (en = ethylenediamine) readily lose their chlorido ligand and transform into the corresponding, more reactive, aquated species.[4–6]

This type of compound has continued to attract attention since it was reported by Morris et al. in 2001 that $[(\eta^6\text{-biphenyl})Ru(en)Cl][PF_6]$ is as cytotoxic to cancer cells as carboplatin.[1] Although the cellular target for (arene)ruthenium compounds and the mechanism underlying their biological effects are not yet known, much of the research has focused on the interaction of these complexes with DNA bases and oligonucleotides.[1,5–10] In the same report Morris et al. described strong and selective binding to G bases on DNA, while no inhibition of topoisomerase I or II was detected. Subsequently, Chen et al. showed that $[(\eta^6\text{-arene})Ru(en)]^{2+}$ complexes exhibit a remarkably high preference for binding to guanine N7.[5,6] Such binding is stabilized by H-bonding between the O6 of G and NH of the en ligand and strong arene–nucleobase stacking when the arene is extended, suggesting a potential DNA-binding mode, involving simultaneous arene intercalation and Ru^{II} coordination.[5,6] Hydrophobic interactions were described both in solution and in the solid state, and it was suggested that it is the flexibility of the arene ligand that allows for simultaneous arene–base stacking and N7-covalent binding. The remarkable site selectivity of the complexes was further demonstrated by Novakova et al. who showed by transcription mapping experiments that in cell-free media the interaction of $[(\eta^6\text{-arene})Ru(en)]^{2+}$ complexes with DNA occurs at G N7.[11] In the same report noncovalent, hydrophobic interaction between the arene ligand and DNA was demonstrated by competitive ethidium displacement.

[a] School of Chemistry, University of Edinburgh, West Mains Road, Edinburgh EH9 3JJ, U.K.

Supporting information for this article is available on the WWW under http://www.eurjic.org or from the author.

Reactions of the (arene)chlorido(ethylenediamine)Ru^{II} complexes with nucleotides appear to involve initial aquation of the arene complexes, and reactions of the aqua complexes with cyclic guanosine monophosphate are faster than those of the chlorido complexes.[4–6] Wang et al. showed that rates of aquation of these (arene)ruthenium anticancer agents are >20× faster than that of cisplatin. The aqua complexes behave as weak acids with pK_a values for the aqua adducts ranging from 7.7 to 8.[4]

In contrast to *cis*-[$PtCl_2(NH_3)_2$], cisplatin, [(η^6-arene)-Ru(en)]$^{2+}$ complexes show little binding to adenine. This is attributable to repulsive interactions between the exocyclic amino group of the base and (en)Ru NH_2 groups.[5,6] Replacing the neutral en by anionic acetyl acetonate as the chelating ligand changes the nucleobase specificity, and the overall affinity for adenosine was demonstrated to be greater than for guanosine.[7] The cytotoxicity of the complexes increases with the size of the arene ring system in the series arene = benzene < *p*-cymene < biphenyl < dihydroanthracene < tetrahydroanthracene which further supports a potential DNA-binding mode, involving simultaneous arene intercalation and Ru^{II} coordination.[2]

Other cytotoxic (arene)Ru complexes of general formula [(η^6-arene)$RuCl_2$(X)] (X = monodentate ligand) have also recently been reported, including 1,3,5-triaza-7-phosphaadamantane (PTA) and imidazole compounds described by Dyson et al.[12–16] These complexes show activity towards the TS/A mouse adenocarcinoma cancer cell line and no apparent cytotoxicity towards HBL-100 human mammary (non-tumor) cell line.[13,14] The cellular target and the mechanism underlying the biological effects for these (arene)ruthenium compounds are also not yet known. The molecules, however, exhibit a pH-dependent DNA damage such that at pH values typical of hypoxic cells DNA is damaged, whereas at pH values characteristic of healthy cells little or no damage is detected.[13,14] The complexes described by Dyson and co-workers may act by a different mechanism from those of general formula [(η^6-arene)-RuCl(X)(Y)]. Loss of the arene is observed in the former complexes, and it has been suggested that single-stranded DNA may wrap around the metal center with formation of multiple coordinative N-donor bonds.[12]

In view of the importance of understanding the biological distribution of (arene)ruthenium compounds, and thus elucidating their mechanism of action, we have tagged them with a small fluorescent probe. Fluorescence microscopy has been widely used to study cellular distribution of organic drugs,[17–19] and recently it has been applied successfully to platinum complexes.[20–24] In the latter case, fluorogenic reporters of different size have been used. These range from large carboxyfluorescein diacetate,[20–22] to medium-size diaminoanthracene[23,24] to small dinitrophenyl derivatives.[20–22] Cellular uptake of labeled compounds is affected by large fluorophores, and it has been suggested that fluorescein-labeled compounds diffuse in and out of the cells and intracellular compartments at a greater rate than the parent compounds.[25]

Owing to these considerations, we have synthesized methylisatoic anhydride (**MIA**) based fluorescent derivatives of (arene)ruthenium complexes and studied their properties. The **MIA** probe was chosen for its relatively small size, a feature that we anticipated might not alter significantly the properties of the complexes. The probe has found wide applications in biochemistry, and it has been used to label a variety of biological substrates ranging from RNA and Ras-like low-molecular-weight GTP-binding proteins to relatively large enzymes like kinases and ATPases.[26–30] We report here the synthesis and characterization of **MIA**-based fluorescent derivatives of (arene)ruthenium complexes (Scheme 1). We have also studied the interaction of complexes **3** and **4** (Scheme 1) with porcine liver esterase (PLE), and we show that esterase-catalyzed hydrolysis reactions can liberate methylisatoic acid (**MIAH**) from complex **3** suggesting a possible use of similar derivatives in esterase-activated Ru-based prodrug delivery systems.

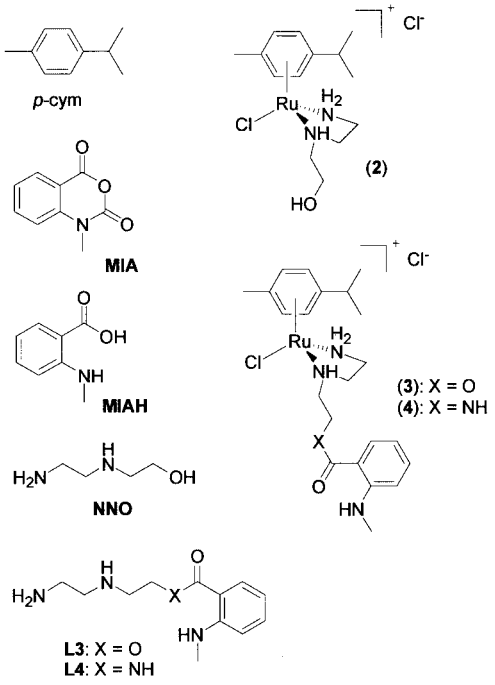

Scheme 1. Structure and abbreviations of ligands, reagents and metal complexes.

Results and Discussion

Synthetic Aspects and General Considerations

Reaction of the dimer [(η^6-*p*-cym)$RuCl_2$]$_2$ (**1**) with 2.2 mol-equiv. of the corresponding ligand afforded the complexes [(η^6-*p*-cym)RuCl(NNO)](Cl) (**2**), [(η^6-*p*-cym)-RuCl(**L3**)](Cl) (**3**) and [(η^6-*p*-cym)RuCl(**L4**)](Cl) (**4**) in good yields (Scheme 2). Complex **2** was first prepared for a direct conjugation reaction with **MIA**. This strategy, however, proved unsuccessful, and we were able to detect only small amounts of **3** by this route. We then proceeded by the organic synthesis of ligands (Scheme 2), and we used **2** as a

standard for comparison with species **3** and **4**. The compounds were characterized by ^{1}H NMR spectroscopy and electrospray ionization mass spectrometry (ESI-MS). The ESI mass spectra of **2**–**4** in water, methanol or CH_3CN provided parent peaks corresponding to the cations. Depending on the cone voltage, peaks corresponding to further loss of HCl were also observed. All spectra confirmed the presence of the expected products.

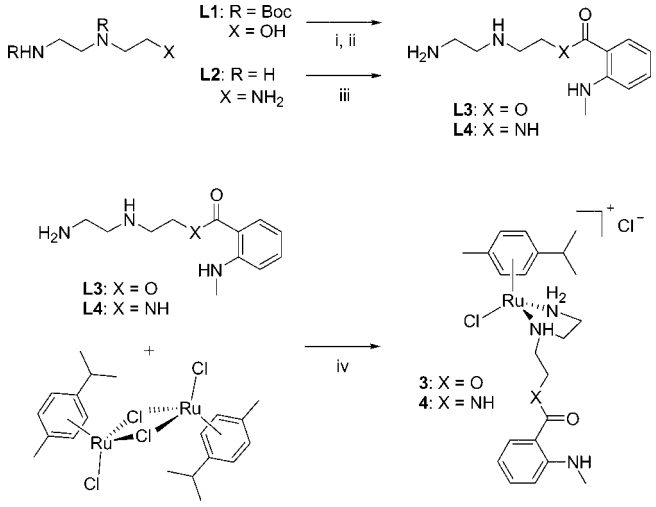

Scheme 2. Synthesis of **MIA**-related ligands and complexes. Conditions: i: **MIA**, CH_3CN, K_2CO_3, room temp. ii: TFA, CH_2Cl_2, room temp. iii: **MIA**, $CHCl_3$, K_2CO_3, room temp. iv: $CHCl_3$, room temp.

Complexes **2**–**4** showed good solubility both in water and organic solvents. The NMR spectra of compounds **3** and **4** in deuteriated chloroform contain peaks between δ = 6.5 and 8.1 ppm that correspond to the aromatic protons of the 2-(methylamino)benzoate/benzamide fragment; aliphatic proton signals are observed between δ = 2.5 and 4.7 ppm. Peaks for arene ligand protons are observed between δ = 5.4 and 5.9 ppm, with the C*H*$(CH_3)_2$ proton displaying a characteristic septet between δ = 1.7 and 2 ppm. Methyl group signals appear at δ ≈ 1.3 ppm. In water, the compounds readily form the corresponding aqua complexes. These are stable at acidic pH*, and no hydroxido species could be detected under these conditions. The pK_a values of the aqua complexes also lie above 7 in agreement with values reported for similar arene species.[4,7] As the pH is raised to within the physiological range (buffered solutions, pH = 7.44) the complexes behave as weak acids forming about 10–15% of the corresponding hydroxido species. Complexes **2** and **3** are stable under these conditions for hours, but **4** slowly undergoes an intramolecular rearrangement following deprotonation at the amide nitrogen atom. This process is described in detail in the following sections. Attempts to obtain X-ray quality crystals of the aqua and hydroxido complexes were unsuccessful, but the chlorido adducts were readily crystallized from organic solvents.

X-ray Crystallography

Crystallographic data are listed in Table 4 and selected bond lengths and angles in Table 1. The structures of the complexes **2**, **4** and **3** are shown in Figures 1, 2 and 3, respectively. All complexes have the familiar pseudo-octahedral "three-legged pianostool" geometry as described previously. Complex **2** crystallizes in space group $P\bar{1}$ with one solvent molecule of methanol and shows disorder in the methyl groups of the isopropyl substituent of *p*-cym. The disorder was modelled by allowing ½ occupancy for each of the four carbon atoms involved. The Cl^- counter anion bridges the hydroxy groups of the solvent molecule and the pendent arm of the chelating ligand through two hydrogen bonds.

Table 1. Selected bond lengths [Å] and angles [°] for cations of **2**, **3** and **4**.[a]

	2	**3**	**4**
Ru–Cl	2.4257(10)	2.4148(8)	2.4149(18)
Ru–N′	2.125(4)	2.132(3)	2.115(6)
Ru–N′′	2.168(3)	2.159(3)	2.142(6)
N′–Ru–N′′	79.48(14)	80.32(10)	79.7(2)
N′–Ru–Cl	83.89(10)	82.71(8)	85.13(17)
N′′–Ru–Cl	86.92(9)	86.88(8)	87.83(17)

[a] N′ and N′′ refer to the primary and secondary amine, respectively, of the chelate ligand.

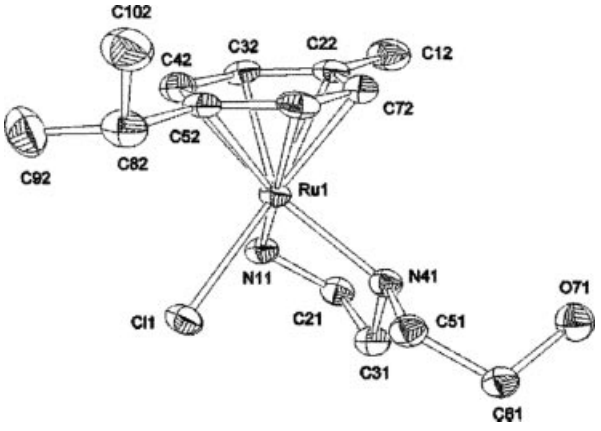

Figure 1. ORTEP diagram and atom numbering scheme for the cation of **2** (50% probability ellipsoids). The H atoms have been omitted for clarity.

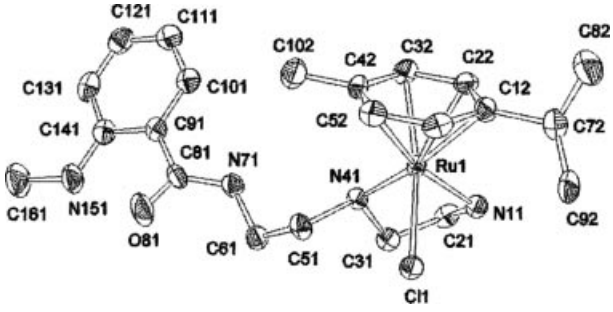

Figure 2. ORTEP diagram and atom numbering scheme for the cation of **4** (50% probability ellipsoids). The H atoms have been omitted for clarity. Two independent molecules of **4** crystallize in the same unit cell; only one is shown.

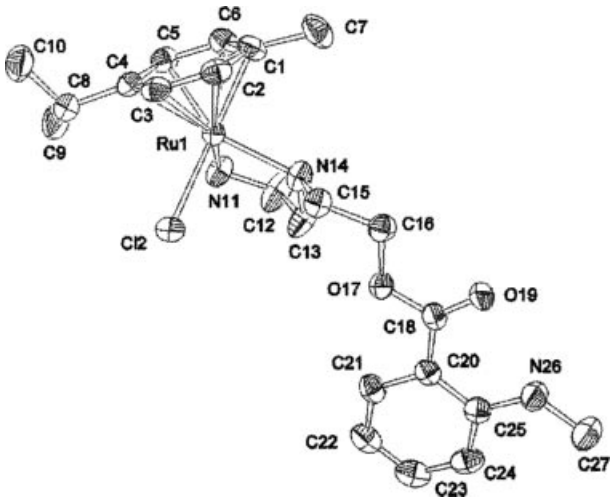

Figure 3. ORTEP diagram and atom numbering scheme for the cation of **3** (50% probability ellipsoids). The H atoms have been omitted for clarity.

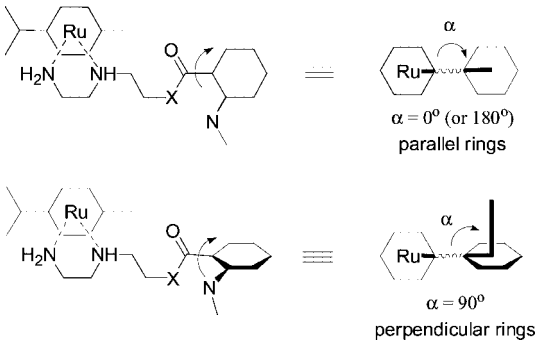

Figure 4. Schematic representation and definition of the angle α.

Complex **4** also crystallized in space group $P\bar{1}$ with two independent molecules in the asymmetric unit. These differ by the relative orientation of the 2-(methylamino)benzamide ring with respect to the aromatic arene ring (see Figure 4). In one molecule the plane defined by the six carbon atoms of the 2-(methylamino)benzamide ring forms an angle α of 28° with the plane of *p*-cym, while in the other molecule the benzamide ring is rotated with an angle α of 47°. Three solvent molecules of chloroform co-crystallize with the complex with two Cl^- counterions completing the content of the asymmetric unit. The counterions form H-bonds with NH and NH_2 groups of the chelating ligand.

In order to obtain crystals of **3**, the Cl^- counterion had to be removed by addition of $AgClO_4$. Thus, complex **3**, as a ClO_4^- salt, crystallized in space group $P2_1/n$. No solvent molecules are present in the asymmetric unit. The ClO_4^- counterion shows disorder in one oxygen atom. In this case also the disorder was modelled by allowing ½ occupancy for each oxygen atom. In this structure the plane defined by the 2-(methylamino)benzoate ring is almost perpendicular to that of the *p*-cym ring (α = 88°, Figure 4).

For structures of the cations of **2**, **3** and **4**, metal–nitrogen and metal–chlorido bonds all fall within normal values (Table 1).[1–7] Bond lengths and distances around the metal coordination sphere are similar (within 3σ) in all three structures indicating that addition of 2-(methylamino)benzoate/benzamide has little effect on the overall coordination of the bidentate chelate. In the crystal structure of the ClO_4^- salt of **3**, short van der Waals contacts are found between *p*-cym hydrogen atoms and the carbonyl oxygen atom and the CH_3NH group of the 2-(methylamino)benzoate fragment of adjacent molecules. These are shown in Figure 5. Such short contacts involving coordinated arenes are becoming increasingly recognized.[31] They have also been observed in [(η^6-*p*-cym)M(acac)Cl] (M = Ru or Os) complexes,[7] and it has been suggested that the weak polarization of arene ring C–H bonds may lead to interactions be-

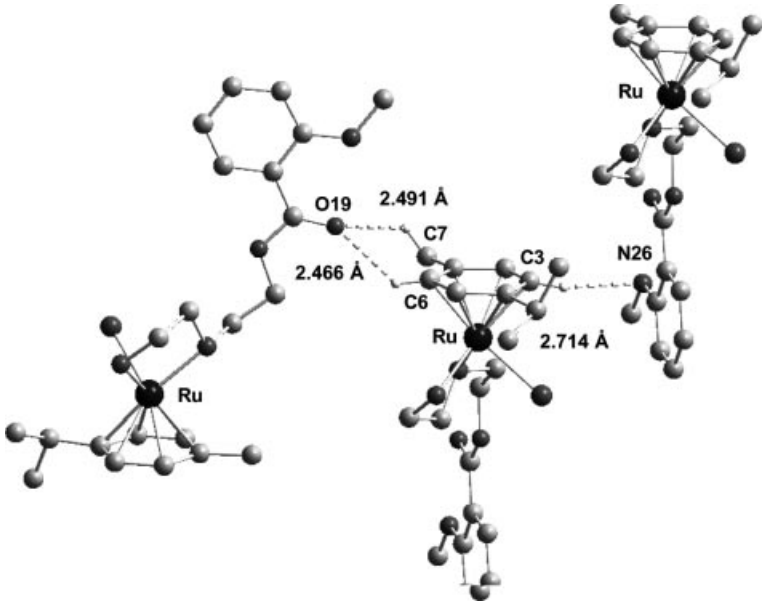

Figure 5. Short contacts involving arene hydrogen atoms of the cation in the crystal structure of **3**.

tween the coordinated arene and H-bond acceptors in biological target sites such as DNA or RNA.[32] It is worth noting that we found no evidence of π-stacking interactions in any of the reported structures.

Complexes **3** and **4** are the first examples of metal complexes with a pendent 2-(methylamino)benzoate/benzamide ring, thus restricting structural comparisons with similar compounds. To the best of our knowledge, the only other instance in which the same fragments have been used in coordination chemistry is in the preparation of Bosnich's type of ligands in complexes investigated for cooperative dimetallic redox reactivity. In those complexes, however, the fragment is part of a larger dinucleating ligand framework.[33–38]

Stability in Aqueous Buffered Solutions

In water the compounds readily form the corresponding aqua complexes which are stable at acidic pH. In a buffered solution (25 mM HEPES, pH = 7.44) the complexes behave as weak acids forming about 10–15% of the corresponding hydroxido species. Complexes **2** and **3** are stable under these conditions for hours, while **4** slowly undergoes an intramolecular rearrangement following deprotonation at the amide nitrogen atom as shown in Scheme 3.

The ^{1}H NMR spectrum of **4** in the buffered solution is shown in Figure 6. After ca. 15 min, three sets of *p*-cym signals were visible in the spectrum of the complex (Figure 6a). The major species is the aqua complex **4a** with *p*-cym resonances at δ = 5.52, 5.67 and 5.72 ppm. The corresponding resonances of the hydroxido species **4b** are shifted upfield to δ = 5.18 and 5.38 ppm. A third set of *p*-cym signals assigned to **4c** appears at δ = 5.15 and 5.30 ppm. Formation of **4c** was clearly evident from the time-dependent evolution of the NMR spectrum. The reaction was complete within 3 h, and the mixture thus obtained was stable for hours under these conditions. Formation of **4c** is accompanied by the appearance of a fourth species (**4d** in Figure 6). The relative integrated intensity of the signals corresponding to **4d** account for about 2% of the total *p*-cym resonances compared to 9% of the hydroxido species **4b** and 89% of **4c**. We tentatively assign these **4d** resonances to an HEPES complex of **4**. Although sulfonates are weak ligands, the assignment is reasonable given the relatively high concentration of the buffer. Moreover, it has been shown that under similar conditions, reactions of (arene)-ruthenium species with nucleotides produce ca. 1.5% of stable phosphate-bound complexes.[6] It is worth noting that the relative concentration of the hydroxido species **4b** remains unchanged during the course of the transformation indicating that the aqua complex **4a** is the reactive species.

Relative to peaks for **4a**, the NHu proton signals suffer a dramatic downfield shift for **4c**. This indicates either a strong interaction of these hydrogen atoms with nucleophilic atoms or a strong deshielding influence of the aromatic ring current of the benzamide fragment; or a combination of both. Related [(η^6-arene)Ru(en)guanine]$^+$ complexes, for example, show stereospecific en NHd bonding with guanine O6, and these species in solution show a downfield shift of the chelate en NHd hydrogen signals of up to 1 ppm compared to the parent aqua complex.[5,6] It is unlikely that the observed shifts result from a partial overlap or π–π stacking of the aromatic rings, but it is possible that the shifts are also a consequence of the ring current generated by the orientation of the benzamide ring. Proton signals of the benzamide fragment show an unusual behaviour. The four non-equivalent resonances collapse into two signals, which might suggest an increased symmetry of the ring. This, however, is not possible as it would imply a complete rearrangement of the ring substituents. Therefore, we assign this to a coincidental overlap of resonances.

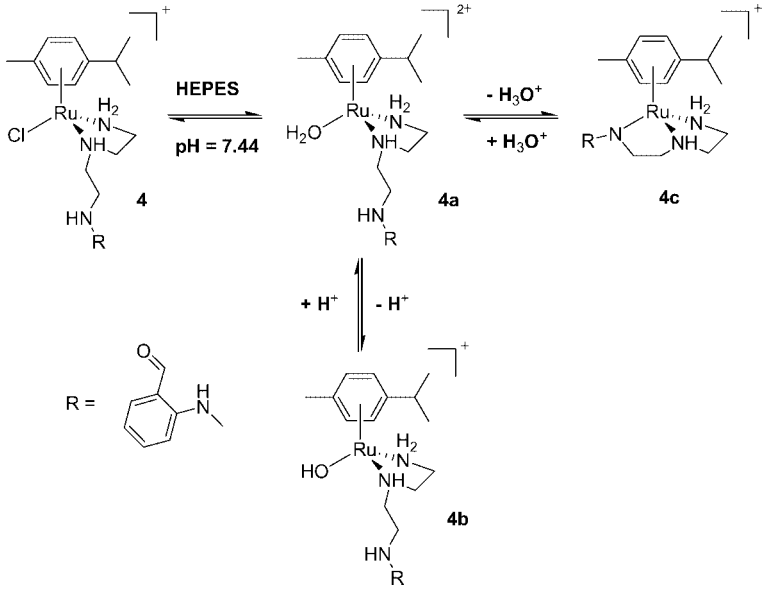

Scheme 3. Hydrolysis of **4** in buffered solution (25 mM HEPES, pH = 7.44).

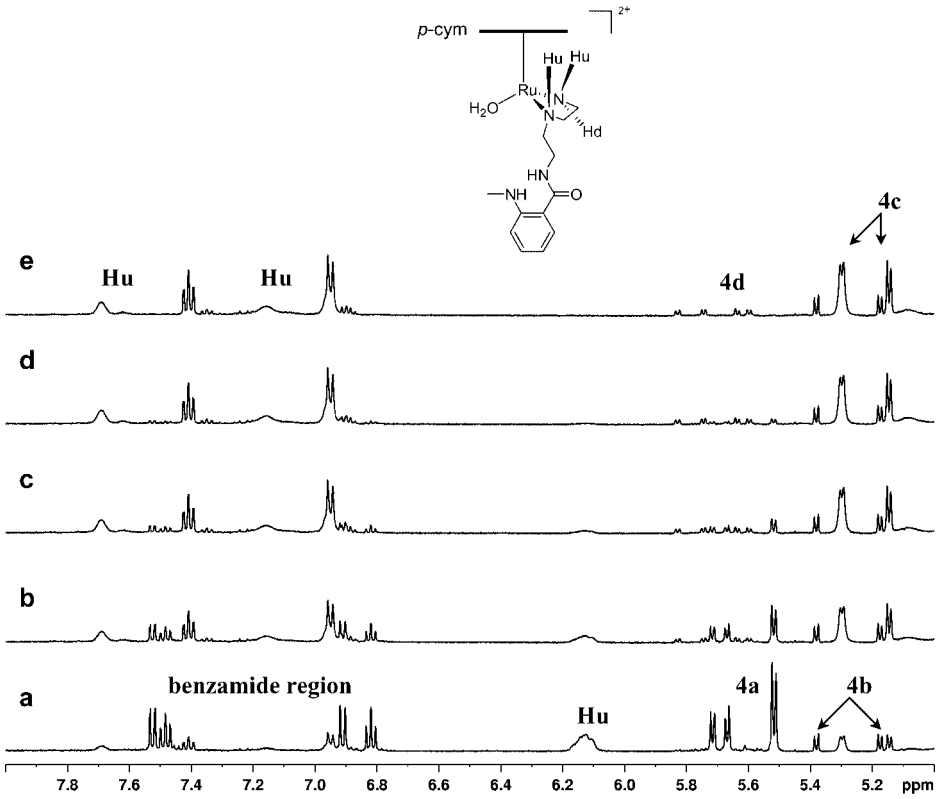

Figure 6. ^{1}H NMR spectrum (δ = 5.1–7.9 ppm) of a 3 mM solution of [(η^6-*p*-cym)Ru(**L4**)Cl]Cl (**4**) in HEPES buffer (25 mM, pH = 7.44). (a) After ca. 15 min; (b–d) 30-min time intervals; (e) after 3 h.

Substitution reactions of the aquated species **4a** are likely to follow the associative interchange mechanism previously described for related complexes. Wang et al. showed that aquation and anation substitution reactions of (arene)Ru species are influenced by steric hindrance of the arene ligand and that the rates of aquation of the halide complexes follow the order Cl ≈ Br > I, consistent with an associative mechanism.[4] Substituents on the *p*-cym ligand exert only minor steric effects when compared to the complexes studied by Wang et al.; however, as a π-acid ligand, *p*-cym depletes electron density on the metal center making it more electropositive. As demonstrated for [(η^6-C_6H_6)-$Ru(H_2O)_3]^{2+}$, this electronic effect makes Ru^{II} behave like an Ru^{III} center in arene species,[39] thus making substitution reactions appear to occur by associative interchange mechanisms.

Changes observed in the NMR spectrum are accompanied by a transition in the UV/Vis spectrum as shown in Figure 7. Soon after dissolution of **4** in the buffer solution (pH = 7.44), the UV/Vis spectrum showed a broad d-d transition between 300 and 360 nm. Within 2 h, a relatively sharp peak at 294 nm replaced this absorption indicating that H_2O is replaced by a ligand which causes a greater splitting of the metal d-orbitals. The intramolecular

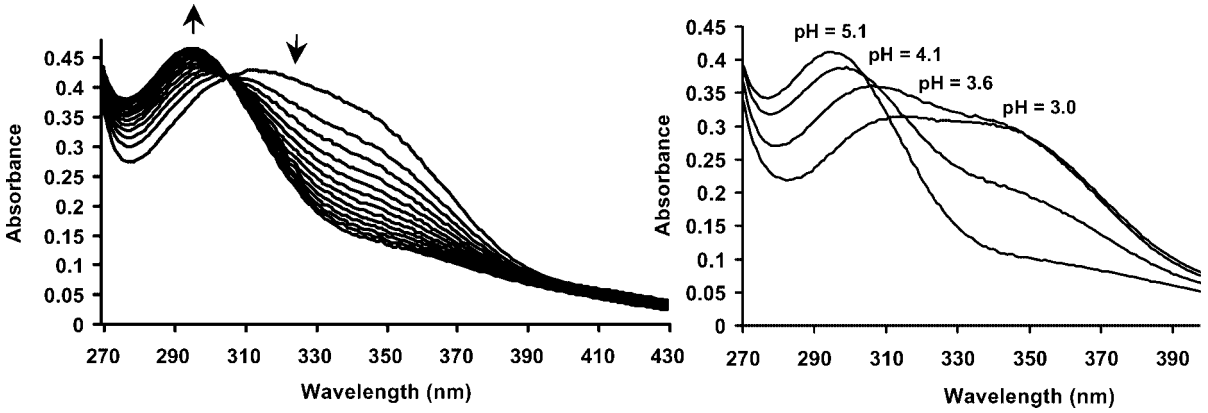

Figure 7. Left: Time evolution of the UV/Vis spectrum of a 0.5 mM solution of **4** (270–430 nm, 25 mM HEPES buffer, pH = 7.44, 5-min time intervals). Right: UV/Vis spectra of **4** at fixed pH values.

rearrangement of **4a** is a pH-dependent reversible process (Figure 7). Aliquots of a stock solution of **4** in water were added to 25 mM HEPES solutions, and the pH was adjusted to different values by addition of HCl. The mixtures were allowed to equilibrate at room temperature for 24 h, and their UV/Vis and ESI-MS spectra were recorded. UV/Vis analysis indicated that **4a** is stable at pH < 3 (Figure 7). Species **4c** began to form at pH ≈ 3.5 and became the predominant species at higher pH values.

ESI-MS analysis confirmed this observation (Supporting Information: Figure S1). At pH < 3.5 only the parent peak corresponding to the cation of **4** is observed ($C_{22}H_{34}ClN_4ORu$: m/z = 507.15, matching the predicted isotope pattern). At higher pH values a second peak corresponding to loss of HCl from the parent cation of **4** was also observed. This peak became the predominant signal at pH > 4.

Geometry Optimization and INDO/S Analysis and Electronic Spectra

The molecular structure of **4c** was also confirmed by theoretical calculations. Molecular structures **B** and **C** were initially modeled from the crystal structure of the cation of **4** (structure **A**) and were optimized at the semiempirical level using default Hyperchem 7.5 INDO/1 functional and basis set. Structures are shown in Figure 8 and selected bond lengths are listed in Table 2. Structure **B** was chosen as a model of **4c**, while **C** (as a **4d** model) was optimized for comparison reasons. The tridentate chelate in **B** is stabilized by hydrogen bonds involving the 2-(methylamino)-benzamide ring and the Hd proton of the primary amine coordinated to the metal center. Compared to **A**, Ru–N distances increase slightly in **B** upon coordination of the deprotonated amide nitrogen atom. These results reflect an increased electron density at the metal center that weakens the σ-donor bonds of the chelate. The opposite effect is calculated for **C**, where Ru–N distances decrease (on average by 0.14 Å) by allowing HEPES to enter the Ru coordination sphere and occupy a coordination site through the sulfonate oxygen atom.

Table 2. Summary of selected INDO/1-optimized bond lengths [pm].

	Ru–NH_2	Ru–NH	Ru–X[a]
Structure **A**	213	215	241
Structure **B**	216	220	199
Structure **C**	200	199	194

[a] X refers to the atom occupying the exchangeable coordination site. Thus, for structure **A**, X = Cl; for structure **B**, X = N; for structure **C**, X = O.

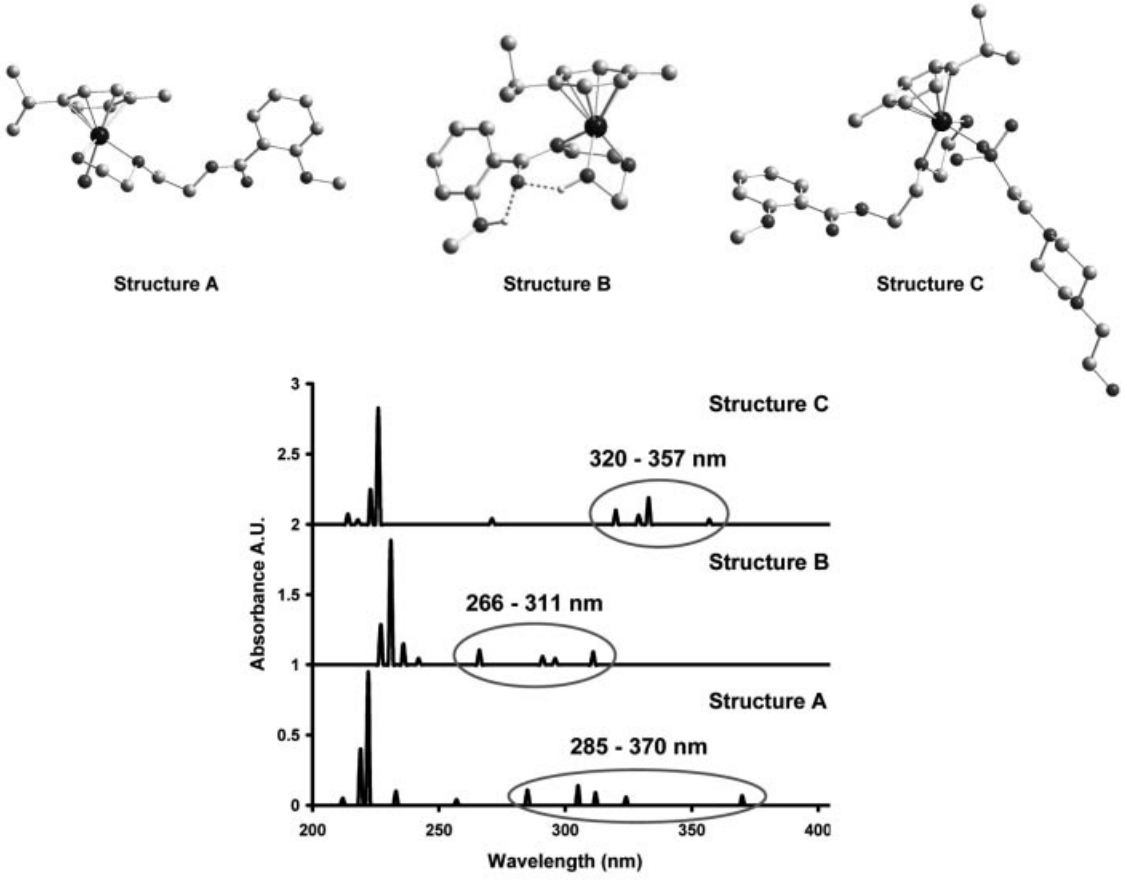

Figure 8. INDO/1-optimized geometry of structure **A** (**4**), **B** and **C** and relative predicted (gas-phase, INDO/S) spectra. Vertical bars are the predicted oscillator strengths and locations of individual computed transitions.

In both **B** and **C** the planarity of the arene ligand is somewhat lost compared to **A**. Both the methyl and the isopropyl group of *p*-cymene are slightly bent out of the plane defined by the six carbon atoms of the *p*-cym aromatic ring. The distortion of the arene is uniform and relatively contained in **C** with both methyl and isopropyl groups deviating from planarity by about 0.06 Å. In **B** the distortion is more pronounced and uneven with the methyl and the isopropyl substituents out of the benzene plane by 0.14 and 0.06 Å, respectively. In **A** the observed deviation is on average 0.04 Å. The net effect of these distortions is clearly visible in the predicted electronic spectra of the complexes discussed below.

Predicted absorptions of structures **A**, **B** and **C** are listed in Table 3, and spectra are shown in Figure 8. Calculations for the electronic spectra are essentially gas-phase, but the Zerner INDO parameters were obtained from solution-phase experimental data and are more likely to predict spectra where the solvent may play an important role.[40–43] In all cases calculated spectra show relatively strong transitions in the 220–235 nm region and a series of peaks of lesser intensity at longer wavelength. Overall the spectra compare well with experimental data. Complexes of the type [(η^6-arene)M(X)(Y)] (M = Ru^{II} or Os^{II}; X, Y = simple σ-donors, monodentate or chelating ligands) show a first band at 300–400 nm which is assigned to a metal d-d transition. A second band appears at around 250 nm with a shoulder at about 225 nm, and these are assigned to a d(M)→π*(X/Y) and to an arene π→π* transition, respectively.[44] The calculated spectra replicate well these features.

The loss of planarity of the arene ligand in **B** and **C** is reflected by a bathochromic shift of the π→π* transition relative to **A** (Figure 8). The degree of shift in energy can be related to the degree of arene distortion in the predicted structures. The shift is more pronounced in **B** (Δ = +9 nm) then in **C** (Δ = +5 nm). These predictions are reasonable because, while most steric effects in organic compounds cause steric inhibition of resonance which determines hypsochromic displacements in the electronic spectrum, geometry distortion tend to cause the opposite effect.[45,46] Distortion of an aromatic system raises the energy of both ground and excited states of the molecule. However, due to the greater antibonding character of the excited states their energies are less affected by distortion. Consequently, it is expected that the UV spectra would show their bands shifted bathochromically with respect to the normal, unstrained compounds of comparable structure and degree of substitution.

With respect to the d-d transition, the experimental UV/Vis spectrum of **4a** at pH = 3 (Figure 7) shows a broad absorption spanning from about 300 to 360 nm. As the pH is raised to 5.1, the transition is blueshifted with $\lambda_{max} \approx$ 294 nm. The predicted spectrum of structure **A** shows five peaks ranging from 285 to 370 nm in close agreement with the experimental spectrum of **4a** at low pH. The same d-d transition suffers two opposite shifts in the calculated spectra of **B** and **C**. A hypsochromic shift in the absorption is predicted for **B** (peaks in the range of 266–311 nm) which is consistent with the replacement of H_2O or Cl^- by the deprotonated amide group with stronger σ-donor character. For **C**, a bathochromic shift is predicted (peaks in the range of 320–357 nm). Of the two optimized structures, **B** shows the closest similarity to the UV/Vis spectrum of **4a** at pH = 5.1 (see Figures 8 and 9). Therefore, in agreement with experimental data, we argue that in 25 mM HEPES at pH = 7.44, **4a** undergoes deprotonation at the nitrogen atom of

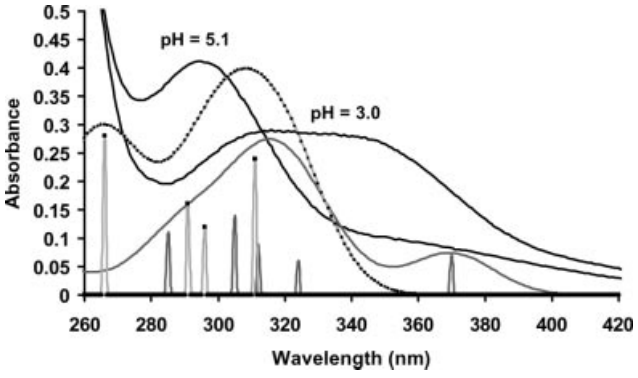

Figure 9. Experimental (black) and predicted (gas-phase, INDO/S) spectra of **4** (dark grey) and of structure **B** (light grey with squares). The vertical bars are the predicted oscillator strengths and locations of individual computed transitions. The oscillator strengths are arbitrarily scaled to match the overall spectra; they retain their correct relative intensity.

Table 3. Predicted spectra for structures **A** (cation of **4**), **B** and **C**.[a]

Structure **A**		Structure **B**		Structure **C**	
Wavenumber ($\times 10^3$ cm^{-1})	Oscillator strength (*f*)	Wavenumber ($\times 10^3$ cm^{-1})	Oscillator strength (*f*)	Wavenumber ($\times 10^3$ cm^{-1})	Oscillator strength (*f*)
27.0	0.07	32.1	0.09	28.0	0.036
30.9	0.06	34.3	0.06	30.0	0.188
32.1	0.09	37.6	0.105	30.4	0.064
32.8	0.14	41.3	0.045	31.3	0.1
35.1	0.11	42.3	0.15	36.9	0.04
38.9	0.04	43.3	0.885	44.3	0.828
42.9	0.1	44.1	0.285	44.8	0.248
45.1	1.09			45.9	0.032
45.7	0.49			46.7	0.072
47.2	0.05				

[a] Only bands for allowed transitions ($f > 0$) are listed. Energies are given to one decimal place since this is only a model system.

the amide group generating a complex with a tridentate chelate encompassing the Ru^{II} center as depicted by structure **B**.

Fluorescence Spectroscopy and PLE-Catalyzed Hydrolysis

In aqueous solutions (pH < 7) compounds **3** and **4** show a photoluminescence response upon excitation at 325 nm. The emission spectra of both compounds show a broad peak centered at around 435 nm. As expected, quenching of fluorescence is observed in the spectra of **3** and **4** compared to the spectra of methylisatoic acid (**MIAH**) and the corresponding free ligands **L3** and **L4** (Figure 10; Supporting Information: Figures S2 and S3). This is due to an internal heavy-atom effect. The quenching of fluorescence by heavy atoms is a phenomenon first identified as "physical quenching" by F. Perrin,[47,48] and it has been the subject of many studies.[49] Heavy atoms in the fluorophore, or in close contact with it, increase the rate of intersystem crossing (ISC) by strengthening spin-orbit coupling,[50,51] as for electronic transitions of heavy atoms. Thus, the decrease of fluorescence yield (radiative transition $S_1 \rightarrow S_0$) is explained by an increase in the probability of the competing $S_1 \rightarrow T_n$ radiationless transition of the fluorophore.

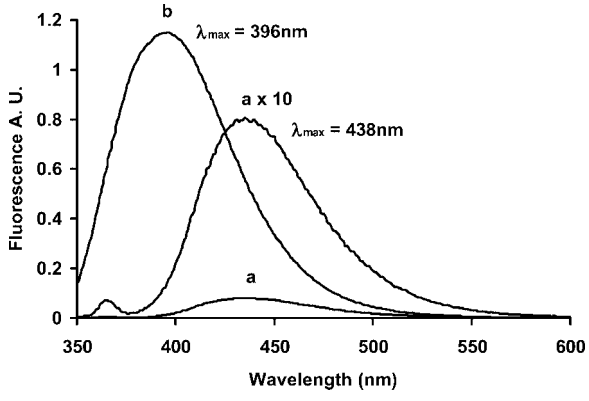

Figure 10. Fluorescence responses (λ_{ex} = 325 nm) of a 7 μM aqueous solution of **4** (a), and of **MIAH** (b).

Complexes **3** and **4** show pH-dependent fluorescence responses (Figure 11) with maxima centered at around neutral pH. Complex **3** shows a local photoluminescence maximum at pH = 6; however, the fluorescence of the sample increases exponentially at pH > 8 due to base-catalyzed hydrolysis of the **L3** ester bond. Under these conditions, the conjugate base of **MIAH** is liberated, and the overall fluorescence of the sample increases. This observation prompted us to study the interaction of compounds **3** and **4** with porcine liver esterase (PLE) in order to determine if the complexes are substrates for this enzyme.

Ester hydrolysis by cytosolic esterases is a common strategy employed to trap photoluminescent organic sensors (most often fluorescein-type sensors) within the cell or to activate organic-based progrugs. Recently, the same strategy has being considered for possible esterase-activated metal-based prodrug delivery systems.[52] Experiments were performed in 25 mM HEPES-buffered solutions at pH = 7.44. Samples of the metal complexes were prepared in the buffer and allowed to equilibrate at room temperature for 5 h. Under these conditions, **3** hydrolyses to form the corresponding aqua (**3a**), hydroxido (**3b**) and HEPES (**3d**) complexes with relative percentage abundances of ca. 84, 14 and 2%, respectively. Complex **4**, on the other hand, is mainly present as the tridentate chelate **4c** following deprotonation at the amide nitrogen atom as described above. After the equilibration period, the enzyme was added and the interactions monitored by ^1H NMR and fluorescence spectroscopy.

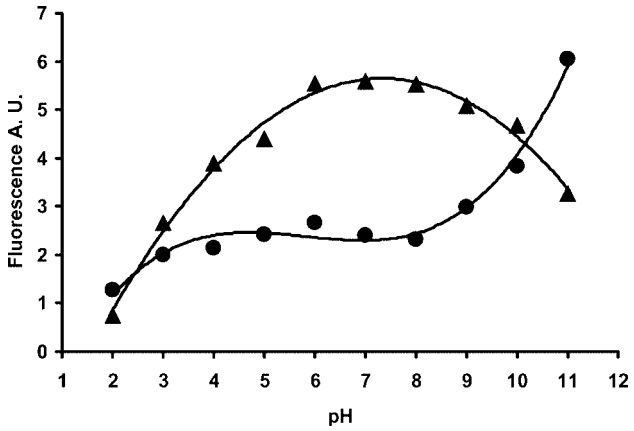

Figure 11. pH-dependent fluorescence responses (λ_{ex} = 325 nm, λ_{em} = 438 nm) of a 7 μM unbuffered aqueous solution of **3** (circles) and of **4** (triangles).

Treatment of **3** with PLE led to an increase in the photoluminescence intensity in its emission spectrum accompanied by a blue shift in the λ_{em} maximum from 438 to 398 nm as shown in Figure 12. The reaction was complete after ca. 150 h of incubation, when no further spectral change could be detected. The hypsochromic shift clearly indicates hydrolysis of the **L3** ester bond and release of free **MIAH**. No change was observed in the fluorescence spectrum of **4** over the same time period. Under our experimen-

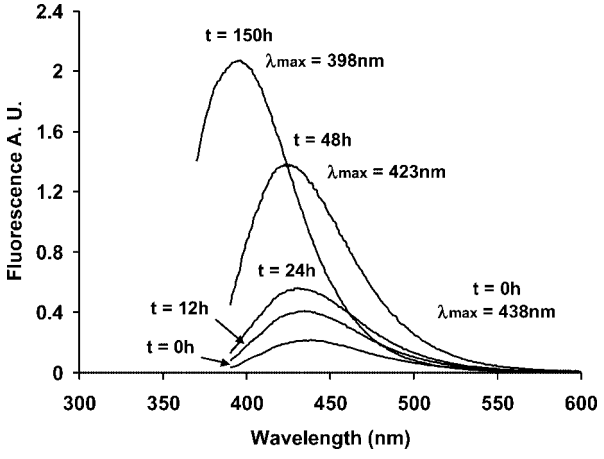

Figure 12. Fluorescence responses (λ_{ex} = 325 nm) of a 10 μM solution of **3** (25 mM HEPES, pH = 7.44) after addition of PLE (7.5 U, incubation at 298 K).

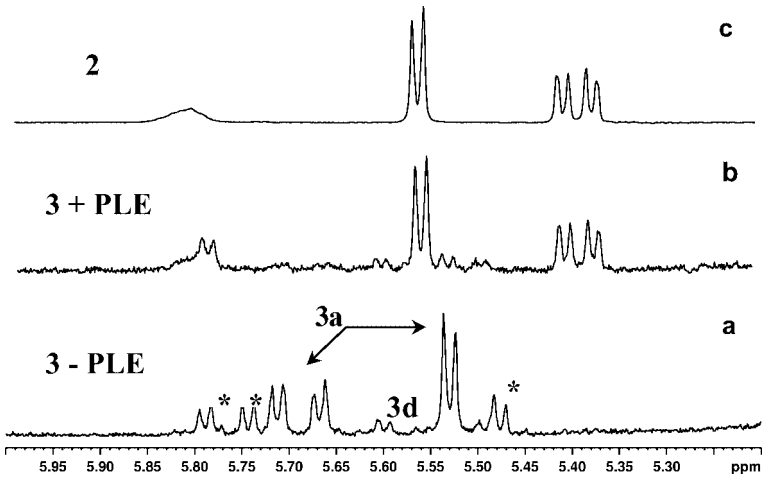

Figure 13. Low-field *p*-cym region of the ^{1}H NMR spectra of a 2 mM solution of **3** in HEPES buffer (25 mM, pH = 7.44); (a) 5 h after dissolution at 298 K, (b) after 1 week incubation with PLE (15 U) at 298 K, (c) *p*-cym peaks of **2** in HEPES buffer (15 min). Asterisks indicate overlapping resonances of **3b** and **3d**.

tal conditions, PLE-catalyzed hydrolysis of the ester bond in **3** appears to be slow ($t_{1/2} \approx 40$ h) when compared to fluorophore-bearing organic molecules.[53] However, we are not aware of comparable examples involving inorganic complexes of the type we have investigated. Platinum complexes prepared by Reedijk and co-workers are all derivatized with fluorogenic reporters through amide bonds.[20–24] Their chemistry has been concentrated on reactions with guanine for comparison with the parent compounds, and they have been studied almost exclusively to elucidate their cellular distribution. Their interactions with cytosolic esterases do not appear to have been investigated.

In order to determine the fate of the ruthenium complex in the PLE-catalyzed hydrolysis of **3**, a millimolar sample of the compound was incubated with the enzyme (HEPES buffer, D_2O solution, pH = 7.44) for 7 d. At the end of the incubation period, a white precipitate was detected and later identified as a 2-(methylamino)benzoate salt. The ^{1}H NMR spectrum of the remaining solution was recorded and compared to the spectra of **2** and **3** in the same buffer. These are shown in Figure 13. The spectrum of **3** in the buffer revealed the presence of three species: the aqua complex (**3a**) as the major adduct, together with the hydroxido (**3b**) and HEPES (**3d**) adducts with overlapping resonances. The species distribution remained unaltered over a period of 5 h. After 1 week, a new single major set of signals was visible (Figure 13b). The peaks show the same resonances (δ = 5.38, 5.41 and 5.56 ppm) as for the *p*-cym peaks of **2** in HEPES (Figure 13c). The experimental evidence clearly indicates that esterase-catalyzed hydrolysis of **3** liberates **MIAH** and generates complex **2**. Thus, although the hydrolysis reaction appears to be slow, the results indicate that **3** is a substrate for the enzyme.

Conclusions

We have synthesized and characterized fluorescent (arene)Ru^{II} complexes of the type [(η^6-arene)RuCl(Z)] (Z = chelating ligand). The compounds show interesting photoluminescent properties and may find some application in fluorescence microscopy studies aimed at elucidation of their cellular trafficking and thus provide new insights into the mechanism of action of this new class of anticancer compounds. Our results show that a fluorogenic reporter may be tagged onto these complexes either through an ester or an amide bond. If the fluorophore is linked through an ester bond, the resulting compounds may be substrates for cytosolic esterases. In this case, esterase-catalyzed hydrolysis of the reporter could potentially alter the fluorescent profile and consequently the resulting (apparent) cellular distribution of the compounds. Derivatization of the compounds through an ester bond, however, might prove useful in the design of esterase-activated Ru-based prodrug delivery systems. This is a common strategy in medicinal chemistry, as it is the case, for example, with capecitabine, an orally available prodrug of 5-deoxy-5-fluorouridine, which has recently come into clinical use for the treatment of breast and colorectal cancers.[54–57] A similar approach focussed on platinum drugs was recently suggested by Lippard.[49] Finally, tagging a reporter (or a prodrug) to (arene)Ru^{II} complexes through an amide linkage is also promising; however, a spacer of proper length (> –[CH_2]$_2$–) must be employed. Our study indicates that if a spacer of only two carbon atoms is used, then the amide nitrogen atom readily undergoes deprotonation under physiological conditions, promoting the formation of a stable five-membered chelate ring.

Experimental Section

Materials: Reagents were purchased from Aldrich and used without further purification. A porcine liver esterase (PLE) suspension was purchased from Fluka and used as supplied. [(η^6-*p*-cym)-$RuCl_2$]$_2$ (**1**) was prepared according to a published procedure.[58,59]

X-ray Crystallography: All diffraction data were collected using a Bruker Smart Apex CCD diffractometer equipped with an Oxford

Table 4. Crystal structure data for complexes **2**, **3** and **4**.

	2	**3**	**4**
Empirical formula	$C_{15}H_{30}Cl_2N_2O_2Ru$	$C_{22}H_{33}Cl_2N_3O_6Ru$	$C_{23.50}H_{35.50}Cl_{6.50}N_4ORu$
Formula mass	442.39	607.50	721.55
Crystal system	triclinic	monoclinic	triclinic
Crystal size [mm]	$0.80 \times 0.33 \times 0.15$	$0.22 \times 0.14 \times 0.08$	$0.75 \times 0.15 \times 0.15$
Space group	$P\bar{1}$	$P21/n$	$P\bar{1}$
V [Å^3]	930.18(14)	2530.47(12)	3035.5(2)
a [Å]	9.0664(8)	10.7840(3)	13.9097(6)
b [Å]	9.8934(8)	10.5940(3)	15.4667(7)
c [Å]	11.1677(9)	22.1650(5)	15.7873(7)
α [°]	109.405(5)	90	80.444(3)
β [°]	90.206(6)	92.1530(10)	69.698(3)
γ [°]	99.447(6)	90	72.812(3)
T [K]	150	150	150
Z	2	4	4
R [$F > 4\sigma(F)$][a]	0.0498	0.0365	0.0804
R_w[b]	0.1384	0.0884	0.1754
GOF[c]	0.7221[d]	0.8676[d]	1.318 [e]
Max/min $\Delta\rho$ [e Å^{-3}]	+1.38/–2.08	+0.98/–0.74	+1.170/–1.219

[a] $R = \Sigma||F_o| - |F_c||/\Sigma|F_o|$. [b] $R_w = [\Sigma w(F_o^2 - F_c^2)^2/\Sigma wF_o^2]^{1/2}$. [c] GOF = $[\Sigma w(F_o^2 - F_c^2)^2/(n - p)]^{1/2}$ (n = number of reflections, p = number of parameters). $F > 4\sigma(F)$. [d] Refinement based on F with ca. 5300 data. [e] Refinement based on F with 12274 data.

Cryosystems low-temperature device operating at 150 K (Table 4). Absorption corrections for all data sets were performed with the multiscan procedure SADABS.[60] Structures were solved by direct methods (SHELXS or SIR92).[61,62] Complexes were refined against F^2 using CRYSTALS (**2** and **3**)[63] or SHELXL (**4**).[61] H-atoms were placed in idealised positions. In **2** the *i*Pr group is rotationally disordered about the pivot carbon atom (C82), and in **3** one O-atom of the perchlorate anion was modelled over two sites. The crystal of **4** was twinned. The diffraction pattern was indexed with two orientation matrices related by a twofold rotation about the (0 1 –1) reciprocal lattice direction (CELL_NOW);[64] reflections from both domains were integrated simultaneously (SAINT)[65] and used in the refinement. The twin scale factor was 0.2811(13). CCDC-634687 (**2**), -634689 (**3**) and -634688 (**4**) contain the supplementary crystallographic data for this paper. These data can be obtained free of charge from The Cambridge Crystallographic Data Centre via www.ccdc.cam.ac.uk/data_request/cif.

NMR Spectroscopy: ^{1}H NMR spectra were acquired with Bruker DMX 500 (^{1}H, 500 MHz) or DPX 360 (^{1}H, 360 MHz) spectrometers using TBI probe-heads equipped with *z*-field gradients. Typically, ^{1}H NMR spectra in D_2O were acquired with water suppression by Shaka's method or with presaturation. ^{1}H NMR chemical shifts were referenced internally to 1,4-dioxane (δ =3.75 ppm) for aqueous solutions, and $CHCl_3$ (δ =7.26 ppm) for [D]chloroform solutions. All data processing was carried out using XWIN-NMR version 2.0 (Bruker U.K. Ltd.).

Mass Spectrometry: Electrospray ionization mass spectra (ESIMS) were obtained with a Micromass Platform II mass spectrometer, and solutions were infused directly. The capillary voltage was 3.5 V, and the cone voltage was varied between 10 and 45 V, depending on sensitivity. The source temperature was 353 K. Mass spectra were recorded in a scan range of m/z = 200–1200 for positive ions.

pH Measurements: pH measurements were carried out using a Corning 240 pH meter equipped with an Aldrich micro-combination electrode calibrated with Aldrich standard buffer solutions of pH = 4, 7, and 10. For NMR samples prepared in D_2O, no correction has been applied for the effect of deuterium on the glass electrode.

Spectroscopic Measurements and Fluorometric Determinations: All glassware was washed sequentially with 20% HNO_3, deionised water, and ethanol before use. Purified water was obtained from a Millipore Milli-Q water purification system. Stock solutions of reagents in water were made up to concentrations of 2 mM and kept at 4 °C in 500-μL aliquots. Portions were diluted to the required concentrations immediately prior to each experiment. Fluorescence and absorption data were measured in water and in HEPES buffer (25 mM, pH = 7.4), prepared with Millipore water. Solutions were stored in clean, dry propylene containers and were filtered before data acquisition. Fluorescence spectra were recorded from 350 to 600 nm. All measurements were performed in triplicate. Fluorescence spectroscopy measurements were performed with Perkin–Elmer LS50B or Edinburgh Instruments FS900 Fluororimeters. Excitation was set to 325 nm and emission was collected through a 350-nm cut-off filter.

Computational Methods: Molecular structures were initially modelled from the crystal structure of the cation of **4** and were optimized at the semiempirical INDO/1 level. A tight self-consistent-field convergence criterion (10^{-6} hartree) was employed in all calculations. The electronic spectra of the complexes were calculated with the INDO/S method in the Zerner implementation[40–42,66] using the Hyperchem (version 7.5) software.[43] The ruthenium and nitrogen atomic parameters of Krogh-Jespersen et al. were used.[67] The overlap weighting factors, $f\sigma$ and $f\pi$, for INDO/S calculations were set at 1.267 and 0.585, respectively, and the number of CISs in the CIS calculations was 1250 (25 occupied and 25 unoccupied orbitals). The optical spectra of these ruthenium complexes were calculated using the SWizard program.[68,69] Half-bandwidths $\Delta_{1/2}$ were assumed to be equal to 3000 cm^{-1}, which is a typical half-bandwidth value for octahedral ruthenium complexes.[70]

Synthetic Procedures

[(η^6-*p*-cym)RuCl(NNO)](Cl) (2): [(η^6-*p*-cym)$RuCl_2$]$_2$ (**1**) (100 mg, 0.16 mmol) was dissolved in $CHCl_3$ (5 mL). To this solution 2.2 mol-equiv. of 2-[(2-aminoethyl)amino]ethanol (**NNO**) was added and the mixture stirred for 12 h. A change in colour of the solution from deep red to pale yellow was observed within 10 s of addition of the ligand to **1**. The yellow precipitate was then collected by filtration, washed with ice-cold $CHCl_3$ and then three times with 5 mL of ice-cold diethyl ether. Yield: quantitative. $C_{14}H_{26}Cl_2N_2ORu$ (410.75): calcd. C 40.98, H 6.39, N 6.83; found C 40.82, H 6.09, N 6.57. ^{1}H NMR (500 MHz, $CDCl_3$): δ = 1.56

(d, 6 H, cymene), 2.43 (s, 3 H, cymene), 2.08 (sept, 1 H, cymene), 2.99 (t, 2 H, CH_2), 3.18 (t, 2 H, CH_2), 3.49 (t, 2 H, CH_2), 3.56 (br., 1 H, NH_2), 4.06 (t, 2 H, CH_2), 5.04 (br., 1 H, NH_2), 6.63 (br., 1 H, OH), 7.33 (br., 1 H,NH) ppm. ESI MS (+ve): m/z = 375 $[M]^+$. Crystals suitable for X-ray diffraction were obtained by slow diffusion of diethyl ether into a methanolic solution of the complex (typically, 5 mg of complex in 250 μL of solvent; diffusion occurred at 4 °C).

***N*,*N*′-Bis(*tert*-butoxycarbonyl)-2-[(2-aminoethyl)amino]ethanol (L1):**[71] To a solution of 2-[(2-aminoethyl)amino]ethanol (50 mmol) in THF/H_2O (1:1) (300 mL), $KHCO_3$ (150 mmol) and *tert*-butoxycarbonyl anhydride (Boc_2O) (120 mmol) were added consecutively at 0 °C. After the reaction mixture had reached room temp., the solution was stirred overnight. The mixture was then acidified to pH = 4 by careful addition of acetic acid at 0 °C and then extracted with CH_2Cl_2 (4 × 200 mL). The combined organic phases were dried (Na_2SO_4) and concentrated under reduced pressure to give **L1** as a viscous colourless oil which crystallized on standing. **L1** was used for the next step without further purification. Yield: 6 g (60%). ^{1}H NMR (360 MHz, $CDCl_3$): δ = 1.44 (s, 9 H, CH_3), 1.47 (s, 9 H, CH_3), 3.32 (m, 2 H, CH_2), 3.37 (m, 4 H, CH_2), 3.74 (m, 2 H, CH_2) ppm. ESI MS (+ve): m/z = 343.37 $[M + K^+]$.

***N*,*N*′-Bis(*tert*-butoxycarbonyl)-2-[(2-aminoethyl)amino]ethyl-2-(methylamino)benzoate (L1′):** Boc-protected 2-[(2-aminoethyl)-amino]ethanol (0.4 g, 1.39 mmol) was dissolved in dried CH_3CN (20 mL). *N*-Methylisatoic anhydride (**MIA**) (0.37 g, 2.08 mmol) was added to this solution. An excess amount of K_2CO_3 (2 g, 27.8 mmol) was added to the above mixture. The mixture was stirred at room temp. for 48 h, during which the reaction progress was monitored by TLC. The desired product was separated from the other possible byproducts and impurities by silica column chromatography using a solvent system of (CH_3OH/CH_2Cl_2, 12:88). The column was eluted with a total of 300 mL of eluent. The fractions obtained were analyzed by ^{1}H NMR spectroscopy, and those containing the desired product were combined. The solvents (CH_3OH/CH_2Cl_2) were removed by rotary evaporation, and the resulting yellow oil was stored at 4 °C for 18 h. During storage, the product spontaneously crystallized into a light yellow solid. Yield: 277 mg (45%). ^{1}H NMR (500 MHz, $CDCl_3$): δ = 1.40 (s, 18 H, CH_3), 2.86 (s, 3 H, CH_3), 3.26 (t, 2 H, CH_2), 3.37 (t, 2 H, CH_2), 3.58 (t, 2 H, CH_2), 4.31 (t, 2 H, CH_2), 4.92 (br., 1 H, NH), 5.15 (br., 1 H, NH), 6.58 (t, 1 H, aromatic), 6.63 (d, 1 H, aromatic), 7.36 (t, 1 H, aromatic), 7.48 (d, 1 H, aromatic) ppm. ESI MS (+ve): m/z = 439.1 $[M]^+$, 338.1 $[M - C_5H_{10}O_2]^+$.

2-[(2-Aminoethyl)amino]ethyl-2-(methylamino)benzoate (L3): Boc deprotection of **L1′** was attained by dropwise addition of 15 mol-equiv. of TFA (1.28 mL, 3.45 mmol) to a solution of **L1′** (0.1 g, 0.23 mmol) in distilled CH_2Cl_2 (10 mL). The mixture was stirred at room temp. for 48 h and was monitored by TLC. The solvents were then removed by rotary evaporation. The crude product was re-dissolved in methanol and purified with the aid of preparative thin layer chromatography (TLC). The desired product was then extracted from preparative TLC silica by re-dissolution in methanol and stirring at room temp. for 18 h. This solution was then filtered under gravity, and all the solvents were removed from the filtrate under vacuum. The product was a dark yellow oil. Yield: 28 mg (51%). $C_{12}H_{19}N_3O_2$ (237.30): calcd. C 60.74, H 8.07, N 17.71; found C 61.03, H 8.04, N 17.38. ^{1}H NMR (500 MHz, D_2O): δ = 2.06 (s, 1 H, CH_3), 3.43 (t, 2 H, CH_2), 3.53 (t, 2 H, CH_2), 3.61 (t, 2 H, CH_2), 4.58 (t, 2 H, CH_2), 6.98 (t, 1 H, aromatic), 7.09 (d, 1 H, aromatic), 7.63 (t, 1 H, aromatic), 8.07 (d, 1 H, aromatic) ppm. ESI MS (+ve): m/z = 238 $[M - H]^+$.

***N*-{2-[(2-Aminoethyl)amino]ethyl}-2-(methylamino)benzamide (L4):** Typically, *N*-(2-aminoethyl)ethane-1,2-diamine (100 mg) was dissolved in $CHCl_3$ (2 mL). To this solution, **MIA** (100 mg) in $CHCl_3$ (2 mL) was added in 0.25-mL portions. Immediately after the addition of **MIA**, a white precipitate appeared. The reaction was allowed to proceed for 2 h. The white precipitate was filtered off, while the $CHCl_3$-soluble fraction was concentrated to about 3 mL and then loaded onto a preparative TLC plate. With 15% CH_3OH in CH_2Cl_2, all the impurities contained in the starting material moved with the front, molecules derivatized with two or three **MIA** moved to the middle of the plate, while **L4** moved only a few cm from the base line. Yield: 38 mg (32%). $C_{12}H_{20}N_4O$ (236.31): calcd. C 60.99, H 8.53, N 23.71; found C 60.23, H 8.40, N 23.69. ^{1}H NMR (500 MHz, $CDCl_3$): δ = 1.75 (br., NH_2), 2.68 (m, 2 H, CH_2), 2.79 (m, 2 H, CH_2), 2.83 (m, 5 H, CH_2 + CH_3), 3.47 (m, 2 H, CH_2), 6.56 (t, 1 H, aromatic), 6.64 (d, 1 H, aromatic), 6.82 (br., NH), 7.30 (t, 1 H, aromatic), 7.36 (2, 1 H, aromatic), 7.47 (br., NH) ppm. ESI MS (+ve): m/z = 259.15 $[M + Na^+]$.

[(η^6-*p*-cym)RuCl(L3)](Cl) (3): Ligand **L3**, (0.032 g, 0.13 mmol), was dissolved in $CH_3OH/CHCl_3$ (20:80) (2.4 mL). This was added dropwise to a solution of $[(\eta^6\text{-}p\text{-cym})RuCl_2]_2$ (**1**) (0.036 g, 0.059 mmol) in $CHCl_3$ (2.8 mL) to prevent any initial precipitation of the ligand. The colour of dimer solution changed from deep red to orange once all of **L3** was added. The mixture was stirred at room temp. for 40 h. During this time, a yellow precipitate developed on the sides of reaction flask, while the colour of the reaction mixture remained unchanged. Further precipitation was obtained by addition of diethyl ether (10 mL). The yellow precipitate was dried under vacuum. Yield: 22 mg (30%). $C_{22}H_{33}Cl_2N_3O_2Ru$ (543.49): calcd. C 48.62, H 6.12, N 7.73; found C 47.98, H 6.07, N 7.91. ^{1}H NMR (500 MHz, $CDCl_3$): δ = 1.38 (d, 6 H, *p*-cymene), 1.74 (sept, 1 H, *p*-cymene), 2.46 (s, 3 H, *p*-cymene), 2.85–3.20 (m, 4 H, CH_2), 3.21 (t, 2 H, CH_2), 4.06 (t, 2 H, CH_2), 4.72 (br., 1 H, NH_2), 5.67–5.78 (dd, 4 H, *p*-cymene), 6.14 (br., 1 H, NH_2), 6.23 (br., 1 H, NH), 6.82 (t, 1 H, aromatic), 6.96 (d, 1 H, aromatic), 7.31 (br., 1 H, OH), 7.53 (t, 1 H, aromatic), 8.04 (d, 1 H, aromatic) ppm. ESI MS (+ve): m/z = 508 $[M]^+$. Crystals suitable for X-ray diffraction were obtained by slow diffusion of pentane into a $CHCl_3$ solution of the complex (5 mg of complex + 2 mg of $NaClO_4$ in 250 μL of solvent; diffusion occurred at room temp.).

[(η^6-*p*-cym)RuCl(L4)](Cl) (4): **1** (44 mg) was dissolved in $CHCl_3$ (3 mL). To this solution 2.2 mol-equiv. of **L4** (38 mg) in $CHCl_3$ (1 mL) was added and the mixture stirred for 48 h. The colour of the solution changed within 1 h from red to orange to olive-green. The reaction was monitored by ^{1}H NMR spectroscopy and stopped when no further change could be observed. Diethyl ether was added to the solution depositing a yellow precipitate which was then collected by filtration and washed with diethyl ether. Yield: 68 mg (78%). $C_{22}H_{34}Cl_2N_4ORu$ (542.51): calcd. C 48.71, H 6.32, N 10.33; found C 48.08, H 5.97, N 9.98. ^{1}H NMR (500 MHz, $CDCl_3$): δ = 1.22 (d, 6 H, CH_3, *p*-cymene), 2.08 (sept, 1 H, *p*-cymene), 2.24, (s, 3 H, CH_3, *p*-cymene), 2.85, (s, 3 H, CH_3), 3.7–2.6, (m, 8 H, CH_2), 5.44 (d, 1 H, *p*-cymene), 5.60 (d, 1 H, *p*-cymene), 5.65 (d, 1 H, *p*-cymene), 5.91 (d, 1 H, *p*-cymene), 6.53 (t, 1 H, aromatic), 6.59 (d, 1 H, aromatic), 7.29 (t, 1 H, aromatic), 7.99 (d, 1 H, aromatic) ppm. ESI MS (+ve): m/z = 507.1 $[M]^+$. Crystals of **4** suitable for X-ray diffraction were obtained by slow diffusion of pentane into a $CHCl_3$ solution of the complex.

Supporting Information (see footnote on the first page of this article). Positive-ion ESI-MS spectra of a solution of **4** in 25 mM HEPES at different pH values; fluorescence response of **L3** and **L4** upon titration of 1.2 mol-equiv. of **1** (Figures S1–S3); ZINDO1/S

parameter files employed in the semiempirical calculations (Table S1).

Acknowledgments

We thank the Swiss National Science Foundation (SNF; fellowship for F. Z.) for the support for this work, and Dr. Abraha Habtemariam and Dr. Ana Maria Pizarro (Edinburgh) for helpful discussions.

[1] R. E. Morris, R. E. Aird, P. del S. Murdoch, H. Chen, J. Cummings, N. D. Hughes, S. Parsons, A. Parkin, G. Boyd, D. I. Jodrell, P. J. Sadler, *J. Med. Chem.* **2001**, *44*, 3616–3621.
[2] R. E. Aird, J. Cummings, A. A. Ritchie, M. Muir, R. E. Morris, H. Chen, P. J. Sadler, D. I. Jodrell, *Br. J. Cancer* **2002**, *86*, 1652–1657.
[3] L. Dadci, H. Elias, U. Frey, A. Hoernig, U. Koelle, A. E. Merbach, H. Paulus, J. S. Schneider, *Inorg. Chem.* **1995**, *34*, 306–315.
[4] F. Wang, H. Chen, S. Parsons, I. D. H. Oswald, J. E. Davidson, P. J. Sadler, *Chem. Eur. J.* **2003**, *9*, 5810–5820.
[5] H. Chen, J. A. Parkinson, S. Parsons, R. A. Coxall, R. O. Gould, P. J. Sadler, *J. Am. Chem. Soc.* **2002**, *124*, 3064–3082.
[6] H. Chen, J. A. Parkinson, R. E. Morris, P. J. Sadler, *J. Am. Chem. Soc.* **2003**, *125*, 173–186.
[7] R. Fernández, M. Melchart, A. Habtemariam, S. Parsons, P. J. Sadler, *Chem. Eur. J.* **2004**, *10*, 5173–5179.
[8] H.-K. Liu, F. Wang, J. A. Parkinson, J. Bella, P. J. Sadler, *Chem. Eur. J.* **2006**, *12*, 6151–6165.
[9] H.-K. Liu, S. J. Berners-Price, F. Wang, J. A. Parkinson, J. Xu, J. Bella, P. J. Sadler, *Angew. Chem. Int. Ed.* **2006**, *45*, 8153–8156.
[10] F. Wang, J. Xu, A. Habtemariam, J. Bella, P. J. Sadler, *J. Am. Chem. Soc.* **2005**, *127*, 17734–17743.
[11] O. Novakova, H. Chen, O. Vrana, A. Rodger, P. J. Sadler, V. Brabec, *Biochemistry* **2003**, *42*, 11544–11554.
[12] A. Dorcier, P. J. Dyson, C. Gossens, U. Rothlisberger, R. Scopelliti, I. Tavernelli, *Organometallics* **2005**, *24*, 2114–2123.
[13] C. Scolaro, A. Bergamo, L. Brescacin, R. Delfino, M. Cocchietto, G. Laurenczy, T. J. Geldbach, G. Sava, P. J. Dyson, *J. Med. Chem.* **2005**, *48*, 4161–4171.
[14] C. Scolaro, T. J. Geldbach, S. Rochat, A. Dorcier, C. Gossens, A. Bergamo, M. Cocchietto, I. Tavernelli, G. Sava, U. Rothlisberger, P. J. Dyson, *Organometallics* **2006**, *25*, 756–765.
[15] C. A. Vock, C. Scolaro, A. D. Phillips, R. Scopelliti, G. Sava, P. J. Dyson, *J. Med. Chem.* **2006**, *49*, 5552–5561.
[16] W. H. Ang, E. Daldini, C. Scolaro, R. Scopelliti, L. Juillerat-Jeannerat, P. J. Dyson, *Inorg. Chem.* **2006**, *45*, 9006–9013.
[17] G. Arancia, A. Calcabrini, S. Meschini, A. Molinari, *Cytotechnology* **1998**, *27*, 95–111.
[18] A. A. Hindenburg, J. E. Gervasoni Jr, S. Krishna, V. J. Stewart, M. Rosado, J. Lutzky, K. Bhalla, M. A. Baker, R. N. Taub, *Cancer Res.* **1989**, *49*, 4607–4614.
[19] A. K. Larsen, A. E. Escargueil, A. Skladanowski, *Pharmacol. Ther.* **2000**, *85*, 217–229.
[20] G. V. Kalayda, G. Zhang, T. Abraham, H. J. Tanke, J. Reedijk, *J. Med. Chem.* **2005**; *48*, 5191–5202.
[21] C. Molenaar, J. M. Teuben, R. J. Heetebrij, H. J. Tanke, J. Reedijk, *J. Biol. Inorg. Chem.* **2000**, *5*, 655–665.
[22] B. A. J. Jansen, P. Wielaard, G. V. Kalayda, M. Ferrari, C. Molenaar, H. J. Tanke, J. Brouwer, J. Reedijk, *J. Biol. Inorg. Chem.* **2004**, *9*, 403–413.
[23] G. V. Kalayda, B. A. J. Jansen, C. Molenaar, P. Wielaard, H. J. Tanke, J. Reedijk, *J. Biol. Inorg. Chem.* **2004**, *9*, 414–422.
[24] G. V. Kalayda, B. A. J. Jansen, P. Wielaard, H. J. Tanke, J. Reedijk, *J. Biol. Inorg. Chem.* **2005**, *10*, 305–315.
[25] M. D. Hall, C. T. Dillon, M. Zhang, P. Beale, Z. Cai, B. Lai, A. P. J. Stampfl, T. W. Hambley, *J. Biol. Inorg. Chem.* **2003**, *8*, 726–732.
[26] K. A. Wilkinson, E. J. Merino, K. M. Weeks, *J. Am. Chem. Soc.* **2005**, *127*, 4659–4667.
[27] T. K. Nomanbhoy, D. A. Leonard, D. Manor, R. A. Cerione, *Biochemistry* **1996**, *35*, 4602–4608.
[28] J. P. Hutchinson, J. F. Eccleston, *Biochemistry* **2000**, *39*, 11348–11359.
[29] A. Y. Jan, E. F. Johnson, A. J. Diamonti, K. L. Carraway III, K. S. Anderson, *Biochemistry* **2000**, *39*, 9786–9803.
[30] S. P. Gilbert, M. L. Moyer, K. A. Johnson, *Biochemistry* **1998**, *37*, 792–799.
[31] D. Braga, F. Grepioni, G. R. Desiraju, *J. Organomet. Chem.* **1997**, *548*, 33–44.
[32] A. F. A. Peacock, A. Habtemariam, R. Fernandez, V. Walland, F. P. A. Fabbiani, S. Parsons, R. E. Aird, D. I. Jodrell, P. J. Sadler, *J. Am. Chem. Soc.* **2006**, *128*, 1739–1748.
[33] A. L. Gavrilova, B. Bosnich, *Chem. Rev.* **2004**, *104*, 349–383.
[34] A. L. Gavrilova, C. Jin Qin, R. D. Sommer, A. L. Rheingold, B. Bosnich, *J. Am. Chem. Soc.* **2002**, *124*, 1714–1722.
[35] C. Incarvito, A. L. Rheingold, A. L. Gavrilova, C. Jin Qin, B. Bosnich, *Inorg. Chem.* **2001**, *40*, 4101–4108.
[36] L. M. Liable-Sands, C. Incarvito, A. L. Rheingold, C. J. Qin, A. L. Gavrilova, B. Bosnich, *Inorg. Chem.* **2001**, *40*, 2147–2155.
[37] C. Incarvito, A. L. Rheingold, C. J. Qin, A. L. Gavrilova, B. Bosnich, *Inorg. Chem.* **2001**, *40*, 1386–1390.
[38] B. Bosnich, *Inorg. Chem.* **1999**, *38*, 2554–2562.
[39] M. Stebler-Rothlisberger, W. Hummel, P. A. Pittet, H. B. Burgi, A. Ludi, A. E. Merbach, *Inorg. Chem.* **1988**, *27*, 1358–1363.
[40] J. Ridley, M. C. Zerner, *Theor. Chim. Acta* **1976**, *42*, 223–236.
[41] M. C. Zerner, G. H. Loew, R. F. Kirchner, U. T. Mueller-Westerhoff, *J. Am. Chem. Soc.* **1980**, *102*, 589–599.
[42] W. P. Anderson, W. D. Edwards, M. C. Zerner, *Inorg. Chem.* **1986**, *25*, 2728–2732.
[43] S. I. Gorelsky, A. B. P. Lever, *J. Organomet. Chem.* **2001**, *635*, 187–196.
[44] Y. Hung, W.-J. Kung, H. Taube, *Inorg. Chem.* **1981**, *20*, 457–463.
[45] J. Kulhánek, S. Böhm, K. Palát, O. Exner, *J. Phys. Org. Chem.* **2004**, *17*, 686–693.
[46] S. Böhm, O. Exner, *Chem. Eur. J.* **2000**, *6*, 3391–3398.
[47] F. Perrin, *J. Phys. Radium* **1926**, *7*, 390–401.
[48] F. Perrin, *J. Chim. Phys.* **1928**, *25*, 531.
[49] S. K. Lower, M. A. El-Sayed, *Chem. Rev.* **1966**, *66*, 199–241.
[50] D. S. McClure, *J. Chem. Phys.* **1949**, *17*, 905–913.
[51] M. Kasha, *J. Chem. Phys.* **1952**, *20*, 71–74.
[52] D. Wang, S. J. Lippard, *Nature Rev. Drug Discovery* **2005**, *4*, 307–320.
[53] C. C. Woodroofe, A. C. Won, S. J. Lippard, *Inorg. Chem.* **2005**, *44*, 3112–3120.
[54] F. Di Costanzo, A. Sdrobolini, S. Gasperoni, *Crit. Rev. Oncol. Hematol.* **2000**, *35*, 101–108.
[55] J. L. Marshall, *Oncology* **2001**, *15*, 41–46.
[56] C. Twelves, M. Boyer, M. Findlay, J. Cassidy, C. Weitzel, C. Barker, B. Osterwalder, C. Jamieson, K. Hieke, *Eur. J. Cancer* **2001**, *37*, 597–604.
[57] M. L. H. Wang, W. K. A. Yung, M. E. Royce, D. E. Schomer, R. L. Theriault, D. F. Wogan, *Am. J. Clin. Oncol.* **2001**, *24*, 421–424.
[58] M. A. Bennett, A. K. Smith, *J. Chem. Soc., Dalton Trans.* **1974**, 233–241.
[59] R. A. Zelonka, M. C. Baird, *Can. J. Chem.* **1972**, *50*, 3063–3072.
[60] G. M. Sheldrick, University of Göttingen, Göttingen, Germany, **2006**.
[61] G. M. Sheldrick, University of Göttingen, Göttingen, Germany, **1997**.
[62] A. Altomare, G. Cascarano, C. Giacovazzo, A. Guagliardi, M. C. Burla, G. Polidori, M. Camalli, *J. Appl. Crystallogr.* **1994**, *27*, 435.
[63] P. W. Betteridge, J. R. Carruthers, R. I. Cooper, K. Prout, D. J. Watkin, *J. Appl. Crystallogr.* **2003**, *36*, 1487.

[64] G. M. Sheldrick, University of Göttingen, Göttingen, Germany, **2005**.
[65] Bruker-Nonius, Bruker-AXS, Madison, Wisconsin, USA, **2006**.
[66] J. Ridley, M. C. Zerner, *Theor. Chim. Acta* **1973**, *32*, 111–134.
[67] K. Krogh-Jespersen, J. D. Westbrook, J. A. Potenza, H. J. Schugar, *J. Am. Chem. Soc.* **1987**, *109*, 7025–7031.
[68] S. I. Gorelsky, SWizard program. http://www.sg-chem.net/swizard/.
[69] P. J. Hay, W. R. Wadt, *J. Chem. Phys.* **1985**, *82*, 270–283.
[70] A. B. P. Lever, *Can. J. Chem.* **2004**, *82*, 1102–1111.
[71] A different synthetic procedure was published: M. T. Schütte, P. Schumacher, C. Unger, R. Mülhaupt, F. Kratz, *Inorg. Chim. Acta* **1998**, *267*, 133–136.

Received: January 31, 2007
Published Online: May 3, 2007

